Radiology

ORIGINAL RESEARCH • GASTROINTESTINAL IMAGING

CT Radiomic Features of Superior Mesenteric Artery Involvement in Pancreatic Ductal Adenocarcinoma: A Pilot Study

Francesca Rigiroli, MD • Jocelyn Hoye, PhD • Reginald Lerebours, MA • Kyle J. Lafata, PhD • Cai Li, PhD • Mathias Meyer, MD • Peijie Lyu, MD • Yuqin Ding, MD • Fides R. Schwartz, MD • Niharika B. Mettu, MD • Sabino Zani Jr, MD • Sheng Luo, PhD • Desiree E. Morgan, MD • Ehsan Samei, PhD • Daniele Marin, MD

From the Departments of Radiology (F.R., K.J.L., M.M., P.L., Y.D., F.R.S., E.S., D.M.) and Radiation Oncology (K.J.L.), Duke University Medical Center, 2301 Erwin Rd, Box 3808, Durham, NC 27710; Multi-Dimensional Image Processing Laboratory, Duke Radiology, Duke University School of Medicine, Durham, NC (F.R., M.M., P.L., Y.D., F.R.S., D.M.); progettoDiventerò, Bracco Foundation, Milan, Italy (F.R.); Carl E. Ravin Advanced Imaging Laboratories (J.H., E.S.), Department of Biostatistics and Bioinformatics (R.L., S.L.), and Duke Electrical and Computer Engineering (K.J.L.), Duke University, Durham, NC; Department of Biostatistics, Yale University, New Haven, Conn (C.L.); Department of Diagnostic and Interventional Radiology and Nuclear Medicine, University Hospital Hamburg-Eppendorf, Hamburg, Germany (M.M.); Department of Radiology, the First Affiliated Hospital of Zhengzhou University, Zhengzhou, Henan Province, People's Republic of China (P.L.); Department of Radiology, Zhongshan Hospital, Fudan University, Shanghai, People's Republic of China (Y.D.); Duke Cancer Center, Duke Health, Durham, NC (N.B.M., S.Z.); and Department of Radiology, University of Alabama at Birmingham, Birmingham, Ala (D.E.M.). Received March 18, 2021; revision requested May 3; revision received June 9; accepted June 17. **Address correspondence to** F.R. (e-mail: *f.rigiroli@gmail.com*).

See also the editorial by Do and Kambadakone in this issue.

Conflicts of interest are listed at the end of this article.

Radiology 2021; 000:1–13 • https://doi.org/10.1148/radiol.2021210699 • Content code: GI

Background: Current imaging methods for prediction of complete margin resection (R0) in patients with pancreatic ductal adenocarcinoma (PDAC) are not reliable.

Purpose: To investigate whether tumor-related and perivascular CT radiomic features improve preoperative assessment of arterial involvement in patients with surgically proven PDAC.

Materials and Methods: This retrospective study included consecutive patients with PDAC who underwent surgery after preoperative CT between 2012 and 2019. A three-dimensional segmentation of PDAC and perivascular tissue surrounding the superior mesenteric artery (SMA) was performed on preoperative CT images with radiomic features extracted to characterize morphology, intensity, texture, and task-based spatial information. The reference standard was the pathologic SMA margin status of the surgical sample: SMA involved (tumor cells ≤1 mm from margin) versus SMA not involved (tumor cells >1 mm from margin). The preoperative assessment of SMA involvement by a fellowship-trained radiologist in multidisciplinary consensus was the comparison. High reproducibility (intraclass correlation coefficient, 0.7) and the Kolmogorov-Smirnov test were used to select features included in the logistic regression model.

Results: A total of 194 patients (median age, 66 years; interquartile range, 60–71 years; age range, 36–85 years; 99 men) were evaluated. Aside from surgery, 148 patients underwent neoadjuvant therapy. A total of 141 patients' samples did not involve SMA, whereas 53 involved SMA. A total of 1695 CT radiomic features were extracted. The model with five features (maximum hugging angle, maximum diameter, logarithm robust mean absolute deviation, minimum distance, square gray level co-occurrence matrix correlation) showed a better performance compared with the radiologist assessment (model vs radiologist area under the curve, 0.71 [95% CI: 0.62, 0.79] vs 0.54 [95% CI: 0.50, 0.59]; $P < .001$). The model showed a sensitivity of 62% (33 of 53 patients) (95% CI: 51, 77) and a specificity of 77% (108 of 141 patients) (95% CI: 60, 84).

Conclusion: A model based on tumor-related and perivascular CT radiomic features improved the detection of superior mesenteric artery involvement in patients with pancreatic ductal adenocarcinoma.

©RSNA, 2021

Online supplemental material is available for this article.

Despite the increasing knowledge of tumor biology, evolving neoadjuvant therapies, and development of interventional and surgical techniques, the outcome for patients with pancreatic ductal adenocarcinoma (PDAC) remains poor (1–4). One of the critical goals for the reduction of tumor recurrence and metastatic disease is the attainment of complete resection (R0) in surgical patients (4–6). As a result, national and international guidelines issued by the National Comprehensive Cancer Network, the European Society for Medical Oncology, and the American Society of Clinical Oncology recommend surgery only in patients with a high probability of R0 resection (4,7,8). This is also a critical variable to stratify patients at higher risk who might benefit from neoadjuvant therapy, including chemotherapy or chemoradiation therapy (4,9,10).

In most institutions, presurgical staging of PDAC relies on dedicated high-quality multidetector row CT of the pancreas (1,4,6). Whereas the role of pancreatic CT has been validated for surgical planning, its ability to help predict the likelihood of achieving R0 margins and resectability remains low (9,11). This task is challenging in the

This copy is for personal use only. To order printed copies, contact *reprints@rsna.org*

Abbreviations

AUC = area under the receiver operating characteristic curve, IQR = interquartile range, PDAC = pancreatic ductal adenocarcinoma, SMA = superior mesenteric artery

Summary

The analysis of tumor-related and perivascular CT radiomic features improved the detection of superior mesenteric artery involvement in patients with pancreatic ductal adenocarcinoma.

Key Results

- In a retrospective study of 194 patients with pancreatic ductal adenocarcinoma, CT radiomic features demonstrated sensitivity of 62% (33 of 53 patients) and specificity of 77% (108 of 141 patients) in the detection of superior mesenteric artery involvement in patients undergoing surgery for pancreatic ductal adenocarcinoma.
- The radiomic model results outperformed the assessment made by expert radiologists in consensus during a multidisciplinary meeting, yielding areas under the curve of 0.71 and 0.54, respectively ($P < .001$).

assessment of vascular involvement, particularly after neoadjuvant therapy due to the confounding effects of therapy-related changes, such as fibrosis and edema (1,9,10,12). The increasing awareness of these limitations is creating uncertainty regarding the appropriate definition of tumor resectability, which may ultimately undermine the role of radiology in the preoperative staging of patients with pancreatic cancer (8–10,12,13).

Previous studies have suggested the utility of radiomics in clinical decision support by providing diagnostic, prognostic, and therapeutic information encrypted in medical images that may serve as a complementary tool to validate clinical and radiologic findings (14–17). Radiomics have been used to differentiate between tumor recurrence and inflammation and to identify specific molecular patterns of pancreatic tumors (18,19). However, previous studies on pancreatic adenocarcinoma have not focused on the preoperative staging or on the characteristics of the peritumoral environment, including the arteries and surrounding perivascular tissue.

The aim of this study was to investigate whether the analysis of tumor-related and perivascular radiomic features can improve preoperative assessment of arterial involvement in patients with surgically proven PDAC.

Materials and Methods

This retrospective study was conducted according to the Health Insurance Portability and Accountability Act and was approved by the institutional review board of Duke University Health System with a waiver of written informed consent because the study design was retrospective and personal health information was deidentified. Siemens Healthineers supported this study by providing the software that was used for segmentation and analysis (Radiomics, version 1.2.0) without any payment. Two authors (E.S., D.M.) dis-

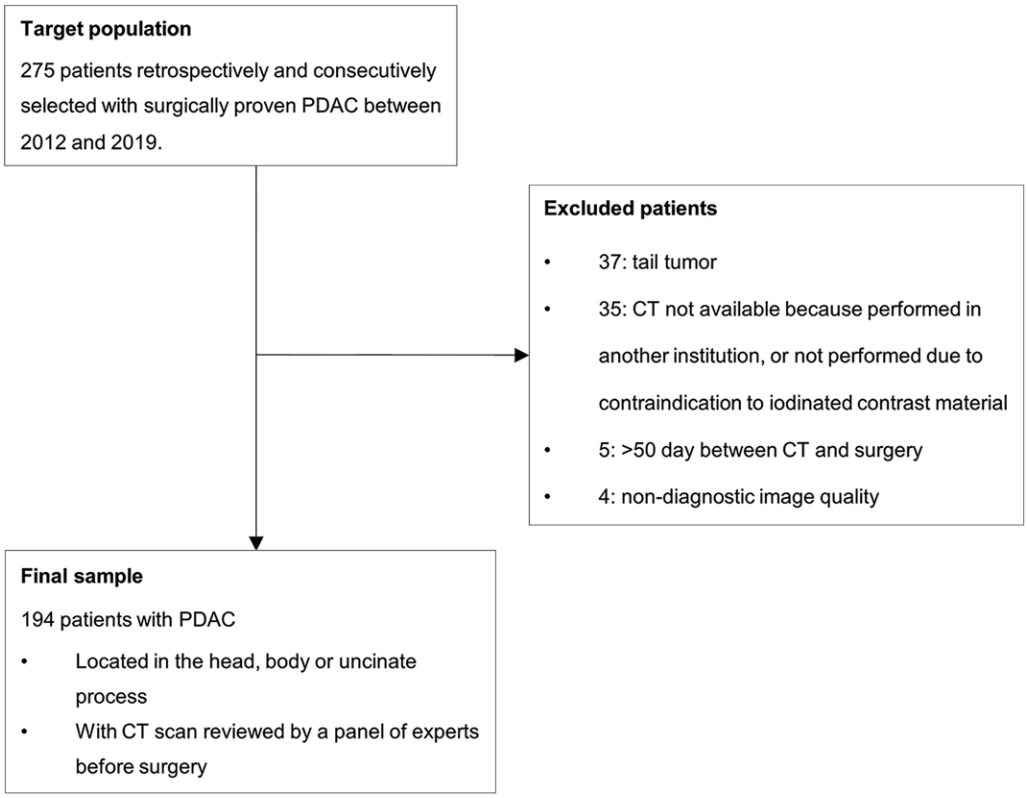

Figure 1: Patient accrual flowchart based on recommended standards for reporting diagnostic performance. PDAC = pancreatic ductal adenocarcinoma.

closed a relationship with Siemens Healthineers. Another author (F.R.), who is not a consultant for or employee of any medical industry, had control of data and information that might have presented a conflict of interest.

The study workflow of the radiomics analysis included image segmentation, feature extraction and selection, and assessment of the regression model performance.

Study Patients

Eligible consecutive patients were retrospectively and consecutively selected from an academic institutional database of the Duke University Health System Department of Surgery (Fig 1). Study data were managed by using REDCap (version 9.1.0, Vanderbilt University Medical Center) electronic data capture tools hosted at Duke University Health System (20). Patients were eligible for our study if they *(a)* underwent curative surgery for PDAC at our institution between 2012 and 2019; *(b)* had a pathologically confirmed diagnosis of PDAC located in the head, body, or uncinate process; and *(c)* had an available preoperative CT scan obtained at our institution. We included patients with and those without neoadjuvant therapy (including chemoradiation therapy and cytotoxic chemotherapy). This represented all the different clinical scenarios evaluated daily by radiologists. Patients were considered ineligible in case of *(a)* nondiagnostic CT image quality (ie, motion- or metal-related artifacts); *(b)* contraindication to iodinated contrast material, such as previous history of anaphylactic reaction or renal failure (serum creatinine level >2.0 mg/dL); or *(c)* the elapse of more than 50 days between the preoperative CT and surgery. Clinical information was collected for each patient, including demographic characteristics (age, sex, race), levels of carbohydrate antigen 19-9 and carcinoembryonic antigen at diagnosis and before surgery, neoadjuvant therapy information, preoperative assessment, and pathologic staging (Table 1).

Table 1: Characteristics of Study Patients

Characteristic	Involved SMA (*n* = 53)	Uninvolved SMA (*n* = 141)	Total (*n* = 194)	*P* Value
Sex				.20 [χ^2 test]
Male	31 (58)	68 (48)	99 (51)	…
Female	22 (42)	73 (52)	95 (49)	…
Median age (y)	66 (58–71)	66 (61–71)	66 (60–71)	.58 [Wilcoxon rank sum test]
Race				>.99 [Fisher exact test]
White	39 (74)	103 (73)	142 (73)	…
Black	11 (21)	29 (21)	40 (21)	…
Native American	1 (2)	4 (3)	5 (3)	…
Asian, unknown, or more than one race or ethnicity	2 (4)	5 (4)	7 (4)	…
Presurgical oncologic assessment*				.15 [Fisher exact test]
Resectable	28 (53)	88 (62)	116 (60)	…
Borderline resectable	19 (36)	47 (33)	66 (34)	…
Locally advanced	6 (11)	6 (4)	12 (6)	…
Neoadjuvant therapy†				.59 [χ^2 test]
Chemoradiation	16 (30)	57 (40)	73 (38)	…
Chemotherapy and chemoradiation	16 (30)	34 (24)	50 (26)	…
Chemotherapy only	8 (15)	17 (12)	25 (13)	…
No neoadjuvant therapy	13 (25)	33 (23)	46 (24)	…
Pathology‡				
Location of primary tumor				.11 [Fisher exact test]
Head	45 (85)	126 (89)	171 (88)	…
Uncinate process	6 (11)	5 (4)	11 (6)	…
Body	2 (4)	10 (7)	12 (6)	…
Median maximum tumor size (cm)	3.1 (2.6–4.0)	3.0 (2.5–4.0)	3.0 (2.5–4.0)	.27 [Wilcoxon rank sum test]
T stage				.73 [Fisher exact test]
T1	2 (4)	9 (6)	11 (6)	…
T2	13 (25)	40 (28)	53 (27)	…
T3	38 (72)	92 (65)	130 (67)	…

Table 1 *(continues)*

Table 1 *(continued)*: Characteristics of Study Patients

Characteristic	Involved SMA (n = 53)	Uninvolved SMA (n = 141)	Total (n = 194)	P Value
N stage				
N0	16 (30)	75 (53)	91 (47)	…
N1	31 (58)	58 (41)	89 (46)	…
N2	6 (11)	8 (6)	14 (7)	…
Grading				.30 [χ^2 test]
Grade 1	5 (9)	24 (17)	29 (15)	…
Grade 2	40 (75)	103 (73)	143 (74)	…
Grade 3	8 (15)	14 (10)	22 (11)	…

Note—Data in parentheses are percentages or interquartile ranges. Data in brackets are the test used to perform statistical analysis. IQR = interquartile range, SMA = superior mesenteric artery.

* Oncologic assessment was performed prospectively during the multidisciplinary meeting and was based on the National Comprehensive Cancer Network guidelines. Source.—Reference 4.

† Neoadjuvant therapy characteristics included *(a)* chemoradiation (ie, standard regimen of four to six cycles of radiation therapy associated with capecitabine or 5-fluorouracil), *(b)* chemotherapy (ie, cytotoxic regimen with gemcitabine plus albumin-bound paclitaxel) followed by chemoradiation, and *(c)* chemotherapy only (ie, Folfirinox or gemcitabine plus albumin-bound paclitaxel).

‡ All the information refers to the pathologic examination of the surgical specimen.

Table 2: CT Scanning Parameters

	Siemens		GE				
Parameter	SOMATOM Definition	SOMATOM Force	Discovery CT750 HD	Light Speed	Revolution	Philips Brilliance	Total
CT parameter							
Tube voltage (kVp)							
100	45	18	NA	NA	NA	NA	63
120	33	1	18	10	9	2	73
140	NA	NA	52	NA	6	NA	58
Tube current (mA)	106–650	106–650		146–701	146–701	273–325	NA
Gantry revolution time	0.5	0.5	0.8	0.8	0.8	0.8	NA
Helical pitch	0.8	0.8	1.375	1.375	1.375	1	NA
Acquisition mode	Helical	Helical	Helical	Helical	Helical	Helical	NA
Section thickness, section interval							
1 mm, 1 mm	52	15	62	3	10	NA	142
2 mm, 2 mm	22	15	7	1		NA	34
3 mm, 3 mm	4	NA	1	6	5	2	18
Kernel	I30f or I31f	Br40d	SOFT	SOFT	SOFT	B	NA
Reconstruction algorithm	SAFIRE S3	SAFIRE S3	ASiR 40%–60%	ASiR 40%–60%	ASiR 40%–60%	iDose^4 level 4	NA
Matrix	512 × 512	512 × 512	512 × 512	512 × 512	512 × 512	512 × 512	NA
$CTDI_{vol}$ median*†	13.78 mGy (9.27–19.58)	13.78 mGy (9.27–19.58)	13.78 mGy (9.27–19.58)	13.78 mGy (9.27–19.58)	13.78 mGy (9.27–19.58)	13.78 mGy (9.27–19.58)	NA
DLP median*†	716.73 mGy × cm(467.61–1048.95)	716.73 mGy × cm (467.61–1048.95)	716.73 mGy × cm (467.61–1048.95)	716.73 mGy × cm (467.61–1048.95)	716.73 mGy × cm (467.61–1048.95)	716.73 mGy × cm (467.61–1048.95)	NA

Table 2 *(continues)*

Table 2: *(continued)*: CT Scanning Parameters

Parameter	Siemens		GE			Philips	Total
	SOMATOM Definition	SOMATOM Force	Discovery CT750 HD	Light Speed	Revolution	Brilliance	
Contrast media injection parameters							
Contrast media	Iopamidol 300 mg iodine/mL (Isovue 300; Bracco Diagnostics)	Iopamidol 300 mg iodine/mL (Isovue 300; Bracco Diagnostics)	Iopamidol 300 mg iodine/mL (Isovue 300; Bracco Diagnostics)	Iopamidol 300 mg iodine/mL (Isovue 300; Bracco Diagnostics)	Iopamidol 300 mg iodine/mL (Isovue 300; Bracco Diagnostics)	Iopamidol 300 mg iodine/mL (Isovue 300; Bracco Diagnostics)	NA
Volume (mL)	175	175	175	175	175	175	NA
Injection rate (mL/sec)	5	5	5	5	5	5	NA
Time of scanning	Automatic bolus tracking with pancreatic parenchymal phase starting 15 sec after threshold (100 HU) was reached in aorta	Automatic bolus tracking with pancreatic parenchymal phase starting 15 sec after threshold (100 HU) was reached in aorta	Automatic bolus tracking with pancreatic parenchymal phase starting 15 sec after threshold (100 HU) was reached in aorta	Automatic bolus tracking with pancreatic parenchymal phase starting 15 sec after threshold (100 HU) was reached in aorta	Automatic bolus tracking with pancreatic parenchymal phase starting 15 sec after threshold (100 HU) was reached in aorta	Automatic bolus tracking with pancreatic parenchymal phase starting 15 sec after threshold (100 HU) was reached in aorta	NA
Saline flush after contrast media	50 mL at 5 mL/sec	50 mL at 5 mL/sec	50 mL at 5 mL/sec	50 mL at 5 mL/sec	50 mL at 5 mL/sec	50 mL at 5 mL/sec	NA

Note.—ASiR = adaptive statistical iterative reconstruction, CTDIvol = volume computed tomography dose index, DLP = dose length product, iDose[4] = fourth generation reconstruction technique, NA = not applicable, SAFIRE = sinogram-affirmed iterative reconstruction.

* Data in parentheses are the interquartile range.

† Source.—Reference 21.

CT Imaging

All multidetector row contrast-enhanced CT examinations were performed by using the institutional routine pancreas protocol. This included a pancreatic parenchymal phase and a portal venous phase. Scanning parameters are summarized in Table 2.

Standard of Care Preoperative Assessment

As part of our standard of care, tumor staging and surgical resectability were prospectively determined at preoperative CT by a multidisciplinary team composed of a fellowship-trained abdominal radiologist (D.M.), a medical oncologist (N.B.M.), three surgical oncologists (including S.Z.), a gastroenterologist, and two interventional radiologists (10–28 years of clinical experience). During the meetings, each patient's information, including medical history, laboratory values, neoadjuvant treatment, and dedicated multiplanar CT reconstruction, was presented to the panel of experts. A consensus agreement between the experts was reached regarding the degree of circumferential vascular involvement by the primary tumor for the celiac artery, superior mesenteric artery (SMA), first arterial jejunal branch, portal vein, superior mesenteric vein, and inferior vena cava. Degree of vascular involvement was characterized as less than or equal to 180° or greater than 180°, according to the National Comprehensive Cancer Network guidelines (4). Based on vascular involvement, pancreatic tumors were categorized as resectable, borderline resectable, or locally advanced, and patients accordingly underwent the appropriate treatment (4,11).

Segmentation

All patient identifiers were removed from the images, and clinical information (demographic characteristics, carbohydrate antigen 19-9 level, carcinoembryonic antigen level, neoadjuvant therapy information, preoperative assessment, and pathologic staging) was blinded to the readers, who did not participate in the multidisciplinary preoperative assessment. The segmentation was performed on images acquired during the pancreatic parenchymal phase of the preoperative CT examination in one readout session for each patient.

Image analysis was performed by a board-certified radiologist with 6 years of experience (F.R.) using prototype segmentation and radiomic feature extraction software (SyngoVia Frontier Radiomics, version 1.2.5; Siemens Healthineers) (22). Based on preliminary testing in 20 patients (Appendix E1, Fig E1 [online]), we restricted our analysis to the assessment of the perivascular tissue around the SMA to minimize the variability related

to manual segmentation. Also, the histopathologic analysis of the surgical sample reported the status of the SMA margin for all the patients, which was not always possible for the other arteries.

The segmentation included the primary PDAC, the SMA, and the perivascular tissue surrounding the SMA (Fig 2). Details on segmentation are available in Appendix E1 (online). To assess the impact of interreader variability of radiomic features and reproducibility of our analysis, the volumetric segmentation of the primary PDAC, SMA, and perivascular tissue was repeated independently for 25 randomly selected patients by three blinded board-certified radiologists (P.L., Y.D., F.R.S.; with 11, 9, and 6 years of experience, respectively) after undergoing a 1.5-hour training session that included familiarization with the segmentation software using test examples.

Radiomic Feature Extraction

Radiomics of the perivascular tissue.—Using the same software, radiomic analysis was performed on the volumes of interest of the perivascular tissue (22). The CT scan and volume of interest were resampled into uniform voxel sizes of 2 × 2 × 2 mm using linear interpolation before subsequent feature extraction to account for differences in pixel spacing (23). All features were calculated using a bin width set to 10 HU (CT attenuation values grouped in intervals of 10 HU) between 1000 HU and 3000 HU (23).

Radiomics of the relationship between the perivascular tissue and the primary tumor.—We used anatomic domain knowledge to build features that study the quantitative relationship between the perivascular tissue and the primary tumor. In total, 20 additional task-based radiomic features were engineered as such (Table 3). The segmentation masks and the CT images were exported into MATLAB software (version 2018b; MathWorks) and resampled into uniform voxels to account for differences in pixel spacing. Six features were derived from texture and intensity comparison between the perivascular tissue and the primary tumor. Fourteen features were based on the spatial relationship between the volumes of interest. In general, spatial image analysis is a useful feature

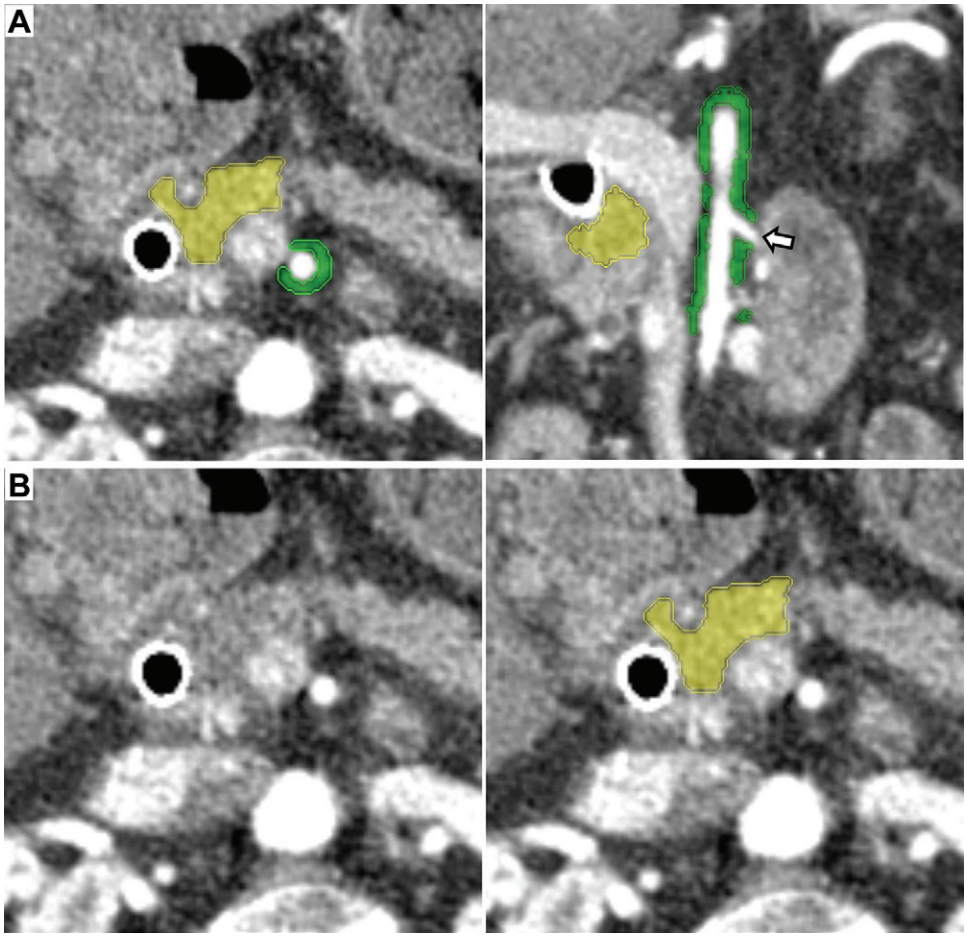

Figure 2: Example of segmentation. A 73-year-old man with pancreatic ductal adenocarcinoma underwent contrast-enhanced CT staging 15 days before surgery, after completing a treatment with chemoradiation (capecitabine plus radiation therapy). The tumor was considered resectable (no contact between tumor and superior mesenteric artery [SMA]) by a consensus of the panel of experts. The pathology report after surgery showed negative SMA margin (R0). **(A)** Segmentation of primary tumor (yellow) and perivascular tissue (green) on pancreatic parenchymal phase CT scan (axial and coronal planes). Arrow shows the exclusion of a small artery from segmentation of the perivascular tissue. **(B)** Semiautomatic segmentation of tumor in axial plane (yellow). (*Fig 2 continues.*)

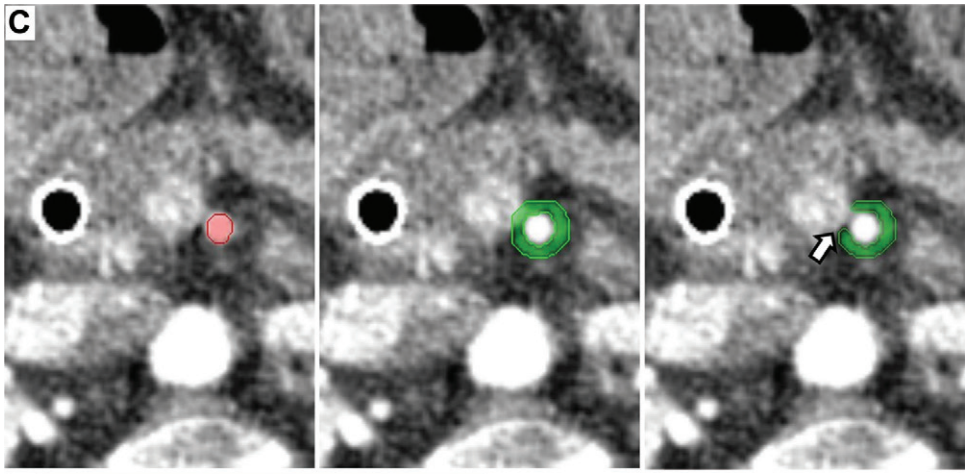

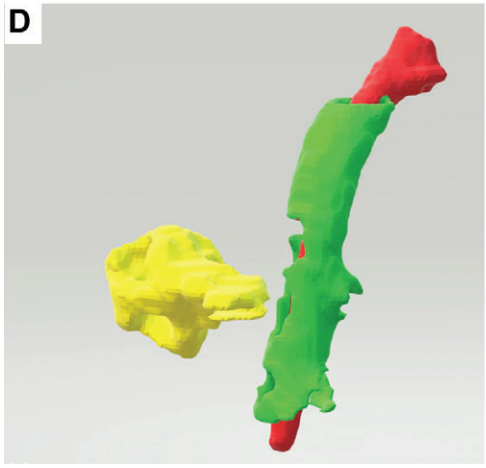

Figure 2: (*continued*) **(C)** Steps followed to segment perivascular tissue (green) in axial plane: segmentation of the superior mesenteric artery (red), creation of the hollow object (green), and manual exclusion of a vein from final segmentation (arrow). **(D)** A three-dimensional rendering of segmentation of tumor (yellow), SMA (red), and perivascular region (green).

Table 3: Radiomics of Relationship between Perivascular Tissue and Primary Tumor

Feature Name	Definition	Mathematical Definition	Reasoning
Mean attenuation difference	Difference in mean, median, maximum, and minimum attenuation, respectively, between tumor and perivascular	F1 = $Mean_{TV} - Mean_{PV}$	The involved cases might have a smaller attenuation difference than those not involved.
Median attenuation difference	…	F2 = $Median_{TV} - Median_{PV}$	…
Maximum attenuation difference	…	F3 = $Maximum_{TV} - Maximum_{PV}$	…
Minimum attenuation difference	…	F4 = $Minimum_{TV} - Minimum_{PV}$	…
Perivascular variation	Standard deviation of the perivascular region normalized by the image noise (as measured by standard deviation of SMA)	F5 = STD_{PV}/STD_{SMAV}	The involved cases might have a more heterogenous perivascular tissue.
Attenuation overlapping	Number of voxels in the perivascular that have attenuation values within range of attenuation values of the tumor	F6 = sum (X), where X is in P and $Minimum_{TV} < X < Maximum_{TV}$	The involved cases might have more perivascular voxels, which have intensity values that overlap with the tumor intensity values.

Table 3 (*continues*)

Table 3: *(continued)*: Radiomics of Relationship between Perivascular Tissue and Primary Tumor

Feature Name	Definition	Mathematical Definition	Reasoning
Attenuation percent overlapping	Overlapping voxels divided by the total number of voxels in the perivascular region	F7 = 100 (F6/N_0), where N_0 is the sum (Y) where Y is in P	The involved cases might have more perivascular voxels, which have intensity values that overlap with the tumor intensity value.
Segmentation overlapping	Number of voxels that are spatially overlapping between the tumor and the perivascular	F8 = sum (position (A) Ç position (B)), where A is in T and B is in P	The involved cases might have tumors that are spatially closer to the perivascular than those not involved.
Center distance	Difference in the spatial center of mass location between the tumor and the perivascular	F9 = sqrt $((X_T\text{-}X_P)^2 + (Y_T\text{-}Y_P)^2 + (Z_T\text{-}Z_P)^2)$, where X_T,Y_T,Z_T are coordinates of COM tumor and X_P, Y_P, and Z_P are coordinates of COM perivascular	The involved cases might have tumors that are spatially closer to the perivascular than those not involved.
Minimum distance	Minimum distance between the perivascular region and the tumor region	F9 = min (sqrt $((X_T\text{-}X_P)^2 + (Y_T\text{-}Y_P)^2 + (Z_T\text{-}Z_P)^2)$), where X_T,Y_T,Z_T are coordinates of all points of the tumor and X_P, Y_P, and Z_P are coordinates of all points of the perivascular	The involved cases might have tumors that are spatially closer to the perivascular than those not involved (Fig 3B).
Closeness	Quantifies the range of minimum distances across image slices	F10 = max ($F9_S$)−min ($F9_S$), where $F9_S$ is the minimum value for each slice	The involved cases might have tumors that are spatially closer to the perivascular than those not involved.
Percent closeness: 10, 20, or 30	This feature describes the consistency of the geometrical closeness between the tumor and perivascular regions across image slices.	F11 = 100 (N/N_S), where N is the number of slices less than (F9+ (10, 20, 30) % of F10) and N_S is the total number of slices	The involved cases might have tumors that are spatially closer to the perivascular than those not involved.
Maximum hugging angle	Overall maximum angle of tumor surrounding (hugging) SMA	F12 = max (H_S), where H_S is the angle of surroundedness of the SMA by the tumor per slice	The involved cases might have tumors that are "hugging" more than those not involved (Fig 3A).
Mean hugging angle	Mean angle of tumor surrounding (hugging) SMA	F13 = mean (H_S), where H_S is the angle of surroundedness of the SMA by the perivascular per slice	The involved cases might have tumors that are "hugging" more than those not involved.
Hugging difference	Maximum hugging angle minus the minimum hugging angle	F14 = max (H_S)−min (H_S), where H_S is the angle of surroundedness of the SMA by the perivascular per slice	The involved cases might have tumors that are "hugging" more than those not involved.
Percent hugging length: 10, 20, or 30	This feature describes the consistency of the hugging of the perivascular region by the tumor across image sections.	F11 = 100 (H/N_S), where H is the number of slices greater than (F12– (10, 20, 30) % of F14) and N_S is the total number of slices	The involved cases might have tumors that are "hugging" more constantly than those not involved.

Note.—The table provides an overview of the task-based radiomic features developed to assess the quantitative relationship between the perivascular tissue and the primary tumor. These features can be classified as spatial (attenuation percent overlapping, segmentation overlapping, center distance, minimum distance, closeness, percent closeness, maximum hugging angle, mean hugging angle, hugging difference, percent hugging length), intensity (mean attenuation difference, median attenuation difference, maximum attenuation difference, minimum attenuation difference, attenuation overlapping), or texture features (perivascular variation). COM = center of mass, P = segmentation of perivascular tissue, PV = intensity values of the perivascular volume, SMA = superior mesenteric artery, SMAV = intensity values of the SMA volume, STD_{PV} = standard deviation of intensity values of the perivascular volume, STD_{SMAV} = standard deviation of intensity values of the SMA volume, T = segmentation of tumor, TV = intensity values of the tumor volume.

engineering approach used to capture the spatial organization or architecture of regions of interest in an image (24). As shown in Figure 3, these features were developed to capture a specific characteristic of the relationship between the tumor and the perivascular tissue, such as the degree of circumferential vascular involvement by the primary tumor (maximum hugging angle) and the closeness between the tumor and the perivascular tissue (minimum distance).

Reference Standard

All patients underwent attempted curative surgical resection, which was performed by a team of two surgeons led by a fel-

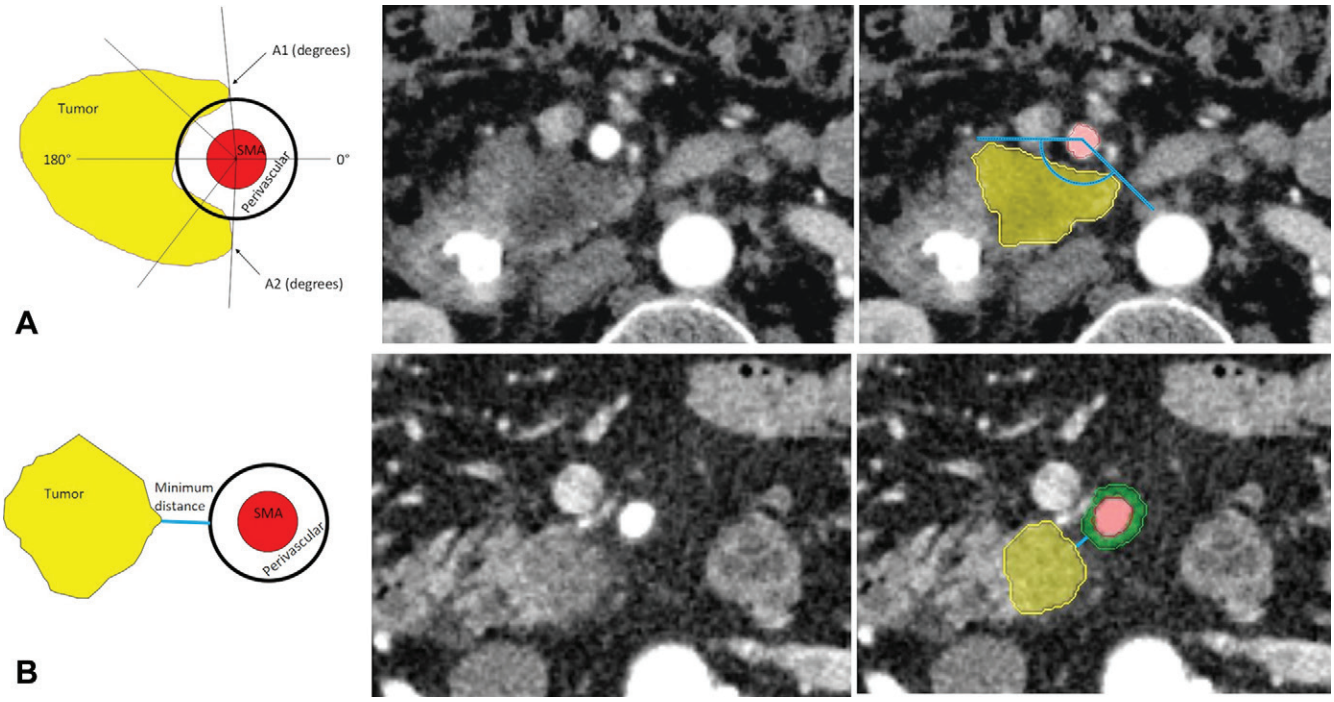

Figure 3: Illustrating example of task-based spatial features between perivascular tissue and tumor. The figure shows a simplification of the spatial features maximum hugging angle **(A)** and minimum distance **(B)**. In **A** and **B** the red segmented object corresponds with the superior mesenteric artery (SMA), the yellow is the tumor, and the green is the perivascular tissue around the SMA (not shown in **A** for simplification). Maximum hugging angle, represented in **A** as the blue angle, refers to the degree of circumferential vascular involvement by the primary tumor. Minimum distance, graphically represented by the blue line in **B**, refers to the minimum distance between the perivascular region and the tumor region. Although the examples are shown in two-dimensional images, it is important to notice that features were calculated on three-dimensional objects.

lowship-trained surgical oncologist who specialized in biliary and pancreatic diseases (clinical experience range, 15–28 years). Surgical samples were analyzed by one fellowship-trained gastrointestinal pathologist with 12 years of experience following the form proposed by the College of American Pathologists (25). Margin identification and specimen orientation were communicated to the pathologist by the surgeon using a different color ink to clearly identify the margins (4,25). An accurate assessment of all margins was performed, and margin involvement was defined as surgical clearance measured in millimeters. Following the most recent National Comprehensive Cancer Network guidelines (4), the status of the SMA margin on the surgical sample was regarded as the reference standard, considering the SMA involved when the tumor cells were identified 1 mm or less from the margin and not involved when they were more than 1 mm from the margin.

Statistical Analysis

Statistical analyses were conducted by a team of statisticians with 3 years (R.L.), 4 years (C.L.), and 13 years (S.L.) of experience using R software (version 4.0.0, the R Foundation) with a threshold for assessing statistical significance set at $\alpha = .05$. Study patient characteristics were summarized by SMA involvement using median and interquartile range (IQR) or frequency and percentage (where appropriate). Differences between SMA involved and SMA not involved groups were compared by using Wilcoxon rank sum test for continuous variables and χ^2 or Fisher exact test for categorical variables.

The following feature selection process was completed for the entire sample and separately for the subset of patients who underwent neoadjuvant therapy. To identify the perivascular features associated with SMA involvement, all the radiomic features were considered as candidate variables for the final logistic regression model. High reproducibility intraclass correlation coefficient greater than or equal to 0.7 and a two-sided univariable Kolmogorov-Smirnov test for SMA involvement were used to select features for the model along with neoadjuvant therapy status, the variable selected for inclusion a priori. To account for multicollinearity, variables with a variance inflation factor greater than five were sequentially removed from the model, starting with the feature with the smallest Kolmogorov-Smirnov test statistic. The performance of the final logistic regression model and the radiologist-led multidisciplinary team were compared by using the DeLong test. Along with the area under the receiver operating characteristic curve (AUC), the sensitivity, specificity, positive predictive value, and negative predictive value were reported, with 95% CIs obtained with the bootstrap technique. The true-positive lesions (SMA with more than 180° of contact with the tumor confirmed to be involved at histopathologic assessment), true-negative lesions (SMA with 180° or less without contact with the tumor confirmed to be not involved at histopathologic assessment), false-positive lesions (SMA with more than 180° of contact with the tumor found to be not involved at histopathologic assessment), and false-negative lesions (SMA with 180° or less or without contact with the tumor found to be involved at histopathologic assessment) for the radiologist assessment and final model were also reported.

Results

Characteristics of Study Patients

Among 275 eligible patients, 81 were excluded, as shown in the study flowchart (Fig 1). The final study cohort consisted of 194 patients with a median age of 66 years (IQR, 60–71 years; age range, 36–85 years), including 95 women with a median age of 65 years (IQR, 61–71 years; age range, 41–81 years) and 99 men with a median age of 66 years (IQR, 59–71 years; age range, 36–85 years). Patients' clinical characteristics are summarized in Table 1. A total of 148 patients (76%) underwent neoadjuvant therapy, including *(a)* chemoradiation alone (ie, standard regimen of four to six cycles of radiation therapy associated with capecitabine or 5-fluorouracil) (73 of 148 patients); *(b)* chemotherapy (ie, cytotoxic regimen with gemcitabine plus albumin-bound paclitaxel) followed by chemoradiation (50 of 148 patients); and *(c)* chemotherapy only (ie, Folfirinox or gemcitabine plus albumin-bound paclitaxel) (25 of 148 patients). The remaining 46 patients (24%) underwent surgical resection without neoadjuvant therapy because of resectable disease at baseline. The median time between the preoperative CT scan and surgery was 24 days (IQR, 15.75–31.25 days; range, 1–50 days).

At pathologic analysis, 171 of 194 (88.1%) tumors were in the pancreatic head, 11 of 194 (5.7%) were in the uncinate process, and 12 of 194 (6.2%) were in the body. The median tumor size for all patients was 3.0 cm (IQR, 2.5–4.0 cm; range, 0.5–7.6). The prevalence of involved SMA was 53 of 194 (27.3%). Most of the patients with involved SMA (n = 48) showed microscopical involvement, with cancer cells less than 1 mm from the margin, while only five patients showed direct involvement. We found no evidence of a difference in clinical characteristics between involved SMA and not involved SMA, except for the N histopathologic staging (P = .01) (Table 1).

Standard of Care Preoperative Assessment

The performance of the radiologist-led multidisciplinary team in the assessment of SMA involvement showed an AUC of 0.54

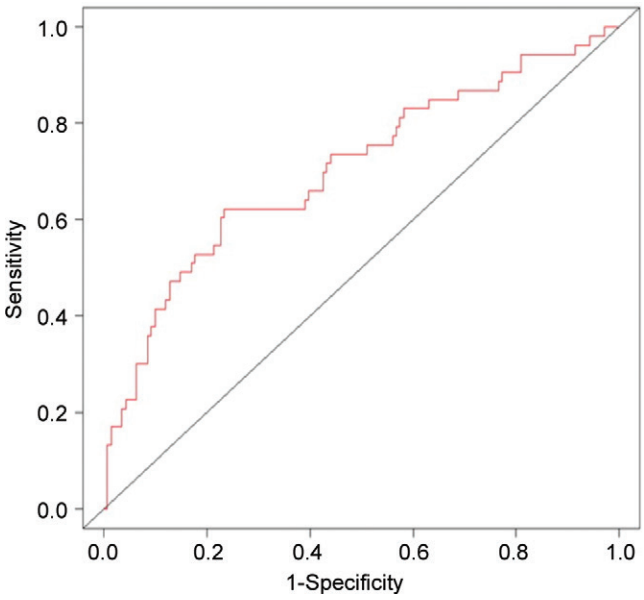

Figure 4: Area under the receiver operating characteristic curve (AUC) of the radiomic model shows mean AUC of the logistic regression model selected was 0.71.

Table 4: Features Included in Final Model after Accounting for Neoadjuvant Therapy

Feature	Odds Ratio	*P* Value
Maximum hugging angle	0.60 (0.38, 0.85)	.01
Maximum diameter	0.89 (0.64, 1.25)	.46
Logarithm robust mean absolute deviation	0.90 (0.65, 1.26)	.51
Minimum distance	1.55 (0.96, 2.61)	.09
Square gray level co-occurrence matrix correlation	0.70 (0.49, 0.99)	.04
Neoadjuvant therapy	1.04 (0.45, 2.33)	.92

Note.—Odds ratios and 95% CIs for modeling selected features using Kolmogorov-Smirnov tests and an intraclass correlation coefficient threshold of 0.7 on not-involved superior mesenteric artery after accounting for neoadjuvant therapy status (n = 194). Data in parentheses are 95% CIs.

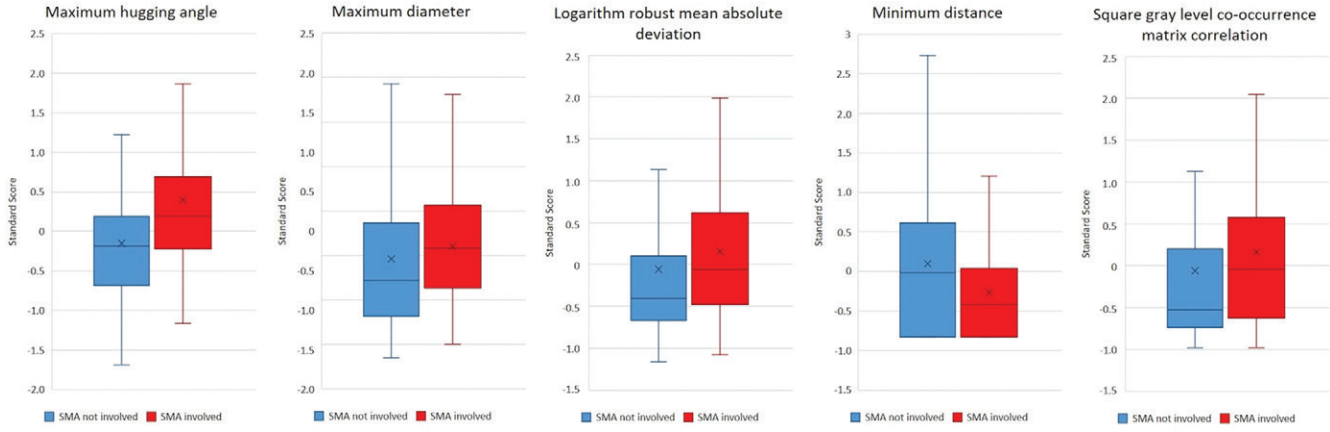

Figure 5: Box plots of the values for the five selected features among all patients with involved superior mesenteric artery (SMA) (red) (n = 53) and all patients with uninvolved SMA outcome (blue) (n = 141). The plots revealed differences in both magnitude and direction (positive and negative) between the two outcomes. Middle "x" = mean; middle line = median.

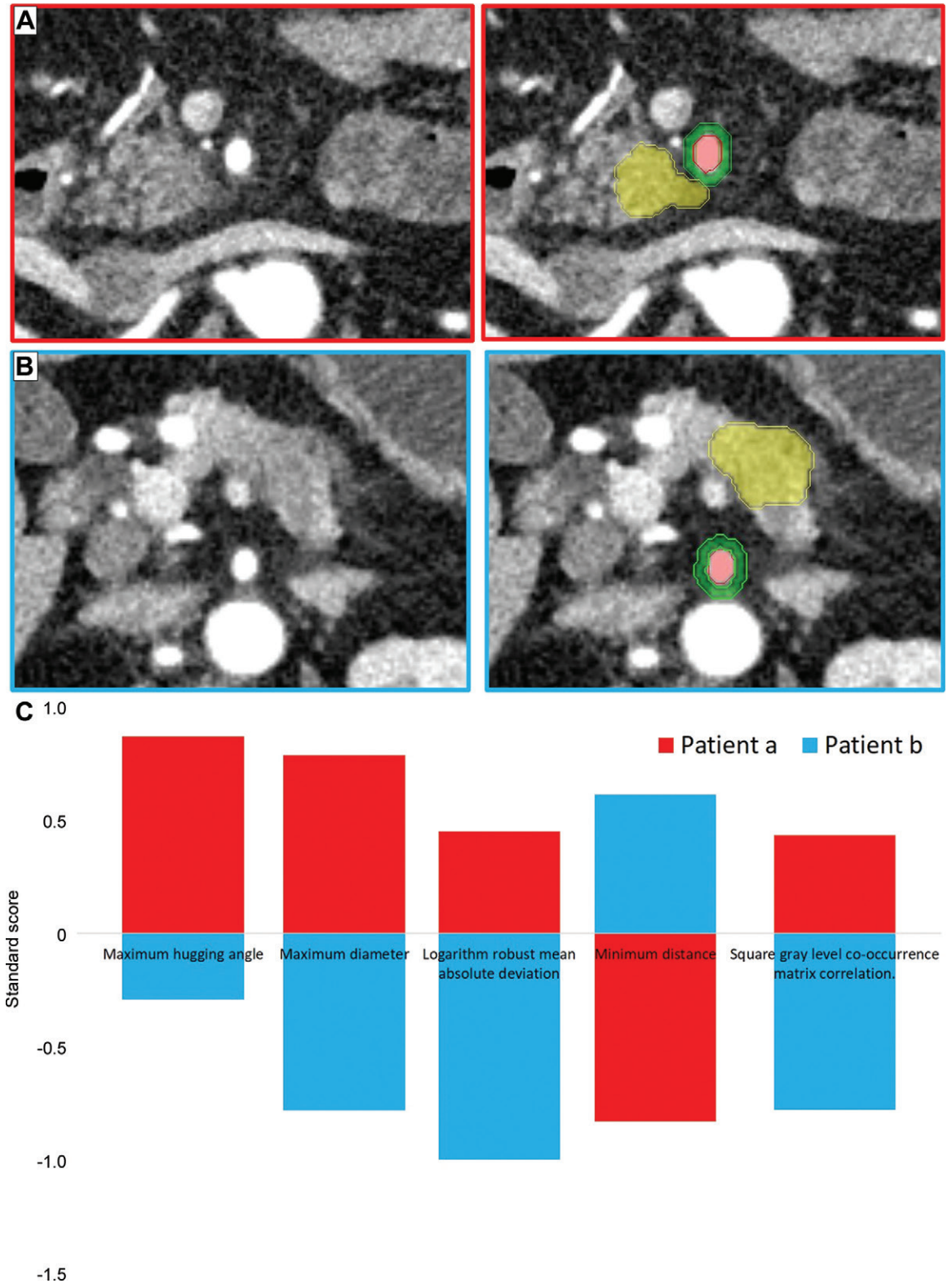

Figure 6: Clinical examples show segmentation of the primary tumor (yellow), superior mesenteric artery (SMA, red), and perivascular tissue (green) in the pancreatic parenchymal phase. **(A)** A 73-year-old man with pancreatic ductal adenocarcinoma underwent contrast-enhanced CT staging 22 days before surgery (axial plane in image) after completing a 5-week treatment with chemoradiation (5-fluorouracil plus radiation therapy). His tumor was considered resectable (less than 180° of contact between tumor and SMA) by consensus of the panel of experts. The pathology report after surgery showed microscopical involvement of the SMA by the tumor. **(B)** A 77-year-old woman with pancreatic ductal adenocarcinoma underwent contrast-enhanced CT staging 8 days before surgery (axial plane in image). Her tumor was considered resectable (no contact between tumor and SMA) by consensus of the panel of experts, and she did not undergo neoadjuvant therapy. The pathology report after surgery showed uninvolved SMA. **(C)** The waterfall plot with values of predictive features for patients A and B showed noticeable differences in both magnitude and direction of the standard score.

(95% CI: 0.50, 0.59). The sensitivity for detection of involved SMA was 11%, (six of 53 tumors) (95% CI: 4, 21), and the specificity was 97% (137 of 141 tumors) (95% CI: 94, 99). The positive predictive value of the multidisciplinary consensus was 60%, and the negative predictive value was 74%.

Logistic Regression Model

A total of 1675 high-throughput radiomic features were extracted from the perivascular volumes of interest, as defined elsewhere *(https://pyradiomics.readthedocs.io/en/latest/features.html)* (Appendix E1 [online]) (26), and 20 additional task-based radiomic features were engineered. Of the 1695 features, 160 features (seven task-based features) had a high reproducibility (intraclass correlation coefficient ≥0.7). Of the reliable features, 11 (three task based) were selected for inclusion in the logistic regression model. Then, six highly correlated features (one task based) were removed, resulting in five radiomic features (maximum hugging angle, maximum diameter, logarithm robust mean absolute deviation, minimum distance, square gray level co-occurrence matrix correlation) included in the final model in addition to neoadjuvant therapy status, which was included a priori.

The model achieved an AUC of 0.71 (Fig 4) (95% CI: 0.62, 0.79), a sensitivity of 62% (33 of 53) (95% CI: 51, 77), and a specificity of 77% (108 of 141) (95% CI: 60, 84). The final model outperformed the radiologist assessment (model AUC, 0.71; 95% CI: 0.62, 0.79 vs radiologist AUC, 0.54; 95% CI: 0.50, 0.59; $P < .001$). The sensitivity of the model at the expected specificity of the radiologist-led multidisciplinary consensus (97%) was 17% (nine of 53) (95% CI: 7, 34). The positive predictive value of the radiomic model was 50%, and the negative predictive value was 84%. The final model included two spatial radiomic features: maximum hugging angle and minimum distance (Fig 3). Similar results were found from the subset analysis for the patients who underwent neoadjuvant therapy (model AUC vs radiologist assessment AUC, 0.73 vs 0.56; $P < .001$) (Appendix E1, Table E1 [online]).

The results of the final logistic model are provided in Table 4. After accounting for the other variables in the model, the odds of SMA noninvolvement were reduced by 40% for each additional unit increase in the standard score (number of standard deviations away from the mean) of maximum hugging angle (odds ratio, 0.60; 95% CI: 0.38, 0.85; $P = .01$). For each unit additional increase in the standard score of square gray level co-occurrence matrix correlation, the odds of SMA noninvolvement were reduced by 30% (odds ratio, 0.70; 95% CI: 0.49, 0.99; $P = .045$). An increased standard score of the feature minimum distance corresponded with higher odds of SMA noninvolvement, although this was not statistically significant (odds ratio, 1.55; 95% CI: 0.96, 2.61; $P = .09$). The model failed to detect an association between neoadjuvant therapy and SMA involvement. The plots in Figures 5 and 6 show noticeable differences in standard score magnitude and direction among the two outcomes for all final selected radiomics features.

Discussion

Imaging methods have shown low performance in predicting complete resection (R0) in patients with pancreatic ductal adenocarcinoma (PDAC) (9,27). This may be because of the complex peripancreatic anatomy and different biologic characteristics of PDAC, further confounded by the challenges of response assessment to neoadjuvant therapy (9). Our study aimed to investigate whether CT radiomic features improve the preoperative assessment of superior mesenteric artery (SMA) tumor involvement in patients with PDAC. We approached the issue of radiomic feature reproducibility (16) by excluding nonreproducible features a priori. The results showed that a model that includes reproducible texture, intensity, and spatial radiomic features explicitly targeting the SMA perivascular tissue outperformed the prospective radiologist-led multidisciplinary consensus of experts (model area under the receiver operating characteristic curve [AUC], 0.71; 95% CI: 0.62, 0.79 vs radiologist AUC, 0.54; 95% CI: 0.50, 0.59; $P < .001$). Similar results were found for the subset analysis of the patients who underwent neoadjuvant therapy, who represented 76% of our final sample (model AUC, 0.73 vs radiologist assessment AUC, 0.56; $P < .001$).

In our study, the radiomic model showed higher negative predictive value than the multidisciplinary assessment in ruling out SMA tumoral involvement defined by a clearance of 1 mm. Our results and previous studies have shown that predicting margin status using only standard CT criteria is challenging (11). Recent investigations have emphasized the need for optimal identification of patients with high likelihood of margin-negative resection, such as with a tumor more than 1 mm from the margin, because it yields a better prognosis compared with patients with positive surgical margin (tumor ≤1 mm to the margin or direct involvement) (4,5). Despite being limited to assessment of the SMA margin, the application of our radiomic model in a clinical setting could help to guide radiologists in predicting margin status.

With the introduction of task-based radiomic features, we exploited the relationships between the primary pancreatic tumor and the perivascular tissue around the SMA. Some studies have used spatial image analysis approaches in the evaluation of lung diseases and hepatic tumors (28,29). Our final model suggested a potential prognostic value in determination of vascular tumor involvement of two spatial features (ie, maximum hugging angle and minimum distance), which provide information about the geometric relationship between the perivascular tissue and the primary tumor. Our model outperformed the results published by Kulkarni et al (30) on the assessment of margin resection status in a study in which radiomics was applied to PDAC but without specifically targeting the perivascular tissue. The findings from our study provide a biologic reasoning behind the radiomic features and represent a step toward a wider applicability and validation of radiomics (16).

The texture feature square gray level co-occurrence matrix correlation represents the heterogeneity of the perivascular tissue around the SMA. After adjusting for neoadjuvant therapy and the other selected features in the final regression model, an increased standard score of square gray level co-occurrence matrix correlation, corresponding to increased heterogeneity, was associated with higher odds of SMA involvement. Based on these findings, we postulate that the perivascular radiomic features may provide additional information by potentially

improving early detection of extrapancreatic perineural invasion in challenging cases of coexistent neoadjuvant therapy-related changes (9,31). Perineural invasion can reflect a particularly aggressive PDAC or the presence of subtle micrometastases, and one of its major pathways involves the superior mesenteric ganglion, which is located near the SMA (31).

Some limitations of our study merit consideration. First, we only included patients with surgically proven PDAC. This allowed for comparison of the radiomic model to the surgical pathologic findings, which is a validated reference standard (32). Second, due to sample size limitation, we could not account for potentially important sources of clinical variability, such as the different regimens of neoadjuvant therapy, CT manufacturer and acquisition parameters, and surgeon experience. Third, features selected for inclusion in the final model had to meet the criterion of an intraclass correlation coefficient greater than or equal to 0.7 and a significant univariable Kolmogorov-Smirnov test based on SMA involvement. Fourth, this preliminary work focused only on the assessment of the SMA involvement. Fifth, the assumption that the ratio of SMA-involved cases reflects the population prevalence of SMA involvement for patients assessed in a clinical setting needs to hold to ensure that the positive predictive value and negative predictive value for the radiologist assessment and final model are generalizable beyond this data set. Sixth, the study was retrospective.

In conclusion, our results suggest that the analysis of tumor-related and perivascular radiomic features improves preoperative assessment of tumor involvement of the superior mesenteric artery in patients with pancreatic ductal adenocarcinoma, a highly challenging task for even experienced multidisciplinary teams, particularly after neoadjuvant therapy. To ensure our model is valid and unbiased, it should be validated in a separate independent data set. Future work may also incorporate more sophisticated modeling techniques, including unsupervised machine learning frameworks (33,34) and deep learning algorithms that fuse radiomics data with other types of clinical data (35). Future studies, preferably prospective ones, are also warranted to investigate the potential application of radiomics on other peritumoral vascular structures and may enable a comprehensive preoperative assessment of resectability.

Acknowledgments: The authors acknowledge Juan Carlos Ramirez-Giraldo, PhD, for contributing expertise in training the radiologists on the software; Susan Whitney, BSRT(R)(N)(CT), and the Duke Multi-Dimensional Image Processing Laboratory for providing assistance with segmentation skills; and Olga R. Brook, MD, for proofreading the manuscript.

Author contributions: Guarantors of integrity of entire study, F.R., D.M.; study concepts/study design or data acquisition or data analysis/interpretation, all authors; manuscript drafting or manuscript revision for important intellectual content, all authors; approval of final version of submitted manuscript, all authors; agrees to ensure any questions related to the work are appropriately resolved, all authors; literature research, F.R., S.Z., E.S.; clinical studies, F.R., M.M., P.L., Y.D., F.R.S., N.B.M., S.Z., D.E.M., E.S.; statistical analysis, R.L., K.J.L., C.L., S.L., E.S.; and manuscript editing, F.R., J.H., R.L., K.J.L., C.L., M.M., Y.D., F.R.S., N.B.M., S.Z., D.E.M., E.S., D.M.

Disclosures of Conflicts of Interest: **F.R.** institution received financial support from Bracco Diagnostics to support work as a research fellow from 2019 to 2021. **J.H.** Siemens Healthineers provided software as part of a research agreement. **R.L.** disclosed no relevant relationships. **K.J.L.** disclosed no relevant relationships. **C.L.** disclosed no relevant relationships. **M.M.** prepared manuscripts for Siemens Healthineers. **P.L.** disclosed no relevant relationships. **Y.D.** disclosed no relevant relationships. **F.R.S.** disclosed no relevant relationships. **N.B.M.** disclosed no relevant relationships. **S.Z.** disclosed no relevant relationships. **S.L.** disclosed no relevant relationships. **D.E.M.** received a one-time consultant fee from GE Healthcare for research review of image quality; institution received equipment to perform image postprocessing research; received a one-time consultant fee from GE Healthcare for educational materials for dual-energy CT. **E.S.** discloses a relationship with the following entities unrelated to the present publication: GE, Siemens, Bracco, Imalogix, 12Sigma, SunNuclear, Metis Health Analytics, Cambridge University Press, and Wiley and Sons. **D.M.** was an associate editor for *Radiology* in 2013; institution received a research grant from Siemens Healthineers.

References

1. Zaky AM, Wolfgang CL, Weiss MJ, Javed AA, Fishman EK, Zaheer A. Tumor-vessel relationships in pancreatic ductal adenocarcinoma at multidetector CT: different classification systems and their influence on treatment planning. RadioGraphics 2017;37(1):93–112.
2. Wagner M, Redaelli C, Lietz M, Seiler CA, Friess H, Büchler MW. Curative resection is the single most important factor determining outcome in patients with pancreatic adenocarcinoma. Br J Surg 2004;91(5):586–594.
3. Ryan DP, Hong TS, Bardeesy N. Pancreatic adenocarcinoma. N Engl J Med 2014;371(11):1039–1049.
4. Tempero MA, Malafa MP, Chiorean EG, et al. Pancreatic adenocarcinoma, version 1.2019. J Natl Compr Canc Netw 2019;17(3):202–210.
5. Strobel O, Hank T, Hinz U, et al. Pancreatic cancer surgery: the new r-status counts. Ann Surg 2017;265(3):565–573.
6. Al-Hawary MM, Francis IR, Chari ST, et al. Pancreatic ductal adenocarcinoma radiology reporting template: consensus statement of the Society of Abdominal Radiology and the American Pancreatic Association. Radiology 2014;270(1):248–260.
7. Ducreux M, Cuhna AS, Caramella C, et al. Cancer of the pancreas: ESMO Clinical Practice Guidelines for diagnosis, treatment and follow-up. Ann Oncol 2015;26(Suppl 5):v56–v68.
8. Khorana AA, Mangu PB, Berlin J, et al. Potentially curable pancreatic cancer: American Society of Clinical Oncology Clinical Practice Guideline update. J Clin Oncol 2017;35(20):2324–2328.
9. Zins M, Matos C, Cassinotto C. Pancreatic adenocarcinoma staging in the era of preoperative chemotherapy and radiation therapy. Radiology 2018;287(2):374–390.
10. Cassinotto C, Mouries A, Lafourcade JP, et al. Locally advanced pancreatic adenocarcinoma: reassessment of response with CT after neoadjuvant chemotherapy and radiation therapy. Radiology 2014;273(1):108–116.
11. Hong SB, Lee SS, Kim JH, et al. Pancreatic cancer CT: prediction of resectability according to NCCN criteria. Radiology 2018;289(3):710–718.
12. Ferrone CR, Marchegiani G, Hong TS, et al. Radiological and surgical implications of neoadjuvant treatment with Folfirinox for locally advanced and borderline resectable pancreatic cancer. Ann Surg 2015;261(1):12–17.
13. Jang JK, Byun JH, Kang JH, et al. CT-determined resectability of borderline resectable and unresectable pancreatic adenocarcinoma following Folfirinox therapy. Eur Radiol 2021;31(2):813–823.
14. Lafata K, Cai J, Wang C, Hong J, Kelsey CR, Yin FF. Spatial-temporal variability of radiomic features and its effect on the classification of lung cancer histology. Phys Med Biol 2018;63(22):225003.
15. Lambin P, Leijenaar RTH, Deist TM, et al. Radiomics: the bridge between medical imaging and personalized medicine. Nat Rev Clin Oncol 2017;14(12):749–762.
16. Tomaszewski MR, Gillies RJ. The biological meaning of radiomic features. Radiology 2021;298(3):505–516.
17. Gillies RJ, Kinahan PE, Hricak H. Radiomics: images are more than pictures, they are data. Radiology 2016;278(2):563–577.
18. Koay EJ, Lee Y, Cristini V, et al. A visually apparent and quantifiable CT imaging feature identifies biophysical subtypes of pancreatic ductal adenocarcinoma. Clin Cancer Res 2018;24(23):5883–5894.
19. Du D, Feng H, Lv W, et al. Machine learning methods for optimal radiomics-based differentiation between recurrence and inflammation: application to nasopharyngeal carcinoma post-therapy PET/CT images. Mol Imaging Biol 2020;22(3):730–738.
20. Harris PA, Taylor R, Thielke R, Payne J, Gonzalez N, Conde JG. Research electronic data capture (REDCap)—a metadata-driven methodology and workflow process for providing translational research informatics support. J Biomed Inform 2009;42(2):377–381.

21. Ria F, Fu W, Hoye J, Segars WP, Kapadia AJ, Samei E. Comparison of 12 surrogates to characterize CT radiation risk across a clinical population. Eur Radiol 2021. Published online February 23, 2021. [Published correction appears in Eur Radiol. 2021 Mar 31. Published online March 31, 2021.]
22. Wels MG, Lades F, Muehlberg A, Suehling M. General purpose radiomics for multi-modal clinical research. Proceedings of SPIE: medical imaging 2019—computer-aided diagnosis. Vol 10950. San Diego, CA: Society of Photo-Optical Instrumentation Engineers, 2019.
23. Cozzi L, Comito T, Fogliata A, et al. Computed tomography based radiomic signature as predictive of survival and local control after stereotactic body radiation therapy in pancreatic carcinoma. PLoS One 2019;14(1):e0210758.
24. Barisoni L, Lafata KJ, Hewitt SM, Madabhushi A, Balis UGJ. Digital pathology and computational image analysis in nephropathology. Nat Rev Nephrol 2020;16(11):669–685.
25. College of American Pathologists. Protocol for the examination of specimens from patients with carcinoma of the pancreas. https://documents.cap.org/protocols/cp-pancreas-exocrine-17protocol-4001.pdf. Published June 2017. Accessed August 8, 2021.
26. van Griethuysen JJM, Fedorov A, Parmar C, et al. Computational radiomics system to decode the radiographic phenotype. Cancer Res 2017;77(21):e104–e107.
27. Cassinotto C, Cortade J, Belleannée G, et al. An evaluation of the accuracy of CT when determining resectability of pancreatic head adenocarcinoma after neoadjuvant treatment. Eur J Radiol 2013;82(4):589–593.
28. Belchi F, Pirashvili M, Conway J, Bennett M, Djukanovic R, Brodzki J. Lung topology characteristics in patients with chronic obstructive pulmonary disease. Sci Rep 2018;8(1):5341.
29. Oyama A, Hiraoka Y, Obayashi I, et al. Hepatic tumor classification using texture and topology analysis of non-contrast-enhanced three-dimensional T1-weighted MR images with a radiomics approach. Sci Rep 2019;9(1):8764.
30. Kulkarni A, Carrion-Martinez I, Jiang NN, et al. Hypovascular pancreas head adenocarcinoma: CT texture analysis for assessment of resection margin status and high-risk features. Eur Radiol 2020;30(5):2853–2860.
31. Chang ST, Jeffrey RB, Patel BN, et al. Preoperative multidetector CT diagnosis of extrapancreatic perineural or duodenal invasion is associated with reduced postoperative survival after pancreaticoduodenectomy for pancreatic adenocarcinoma: preliminary experience and implications for patient care. Radiology 2016;281(3):816–825.
32. Bluemke DA, Moy L, Bredella MA, et al. Assessing radiology research on artificial intelligence: a brief guide for authors, reviewers, and readers—from the *Radiology* editorial board. Radiology 2020;294(3):487–489.
33. Lafata KJ, Chang Y, Wang C, et al. Intrinsic radiomic expression patterns after 20 Gy demonstrate early metabolic response of oropharyngeal cancers. Med Phys 2021. 10.1002/mp.14926. Published online May 6, 2021.
34. Lafata KJ, Zhou Z, Liu JG, Yin FF. Data clustering based on Langevin annealing with a self-consistent potential. Q Appl Math 2019;77(3):591–613.
35. Huang SC, Pareek A, Seyyedi S, Banerjee I, Lungren MP. Fusion of medical imaging and electronic health records using deep learning: a systematic review and implementation guidelines. NPJ Digit Med 2020;3(1):136.